

# Temperature Evolution of the Pseudogap State in the Infra-Red Response of Underdoped $\text{La}_{2-x}\text{Sr}_x\text{CuO}_4$

T. Startseva<sup>(1)</sup>, T. Timusk<sup>(1)</sup>, A.V. Puchkov<sup>(2)</sup>, D.N. Basov<sup>(3)</sup>, H.A. Mook<sup>(4)</sup>, M. Okuya<sup>(5)</sup>, T. Kimura<sup>(5)</sup>, and K. Kishio<sup>(5)</sup>

<sup>(1)</sup> Department of Physics and Astronomy, McMaster University  
Hamilton, Ontario, CANADA L8S 4M1

<sup>(2)</sup> Department of Applied Physics, Stanford University, Stanford, CA 94305

<sup>(3)</sup> Department of Physics, University of California San-Diego, La Jolla, CA 92093

<sup>(4)</sup> Oak Ridge National Laboratory, Oak Ridge, Tennessee 37831

<sup>(5)</sup> Department of Applied Chemistry, University of Tokyo, Tokyo 113, Japan

The  $ab$ -plane optical spectra of two single crystals of underdoped  $\text{La}_{2-x}\text{Sr}_x\text{CuO}_4$  were investigated. The reflectivity of  $\text{La}_{1.87}\text{Sr}_{0.13}\text{CuO}_4$  has been measured in the frequency range  $30 - 9,000 \text{ cm}^{-1}$  ( $0.004 - 1 \text{ eV}$ ) both parallel and perpendicular to the  $\text{CuO}_2$  planes, whereas  $\text{La}_{1.86}\text{Sr}_{0.14}\text{CuO}_4$  was studied only in the  $ab$ -plane. The extended Drude model shows that the frequency-dependent effective scattering rate  $1/\tau(\omega, T)$  is strongly suppressed below the high-frequency straight-line extrapolation, a signature of the pseudogap state. This suppression can be seen from temperatures below the superconducting transition up to 400 K. In the case of underdoped LSCO the straight-line extrapolation is temperature independent below 200 K, whereas above 200 K there is a strong temperature dependence of the high-frequency  $1/\tau(\omega, T)$ . The out-of-plane direction is also examined for evidence of the pseudogap state.

PACS numbers: 74.25.Gz, 74.7.2.Dn, 74.72.Jt, 74.72.-h, 78.20.Ci

The presence of a pseudogap in the normal state of underdoped high temperature superconductors is by now widely accepted. [1] The strongest evidence for the pseudogap state comes from recent measurements of angle resolved photoemission spectra [2] as well as vacuum tunneling [3]. However, these techniques both demand extremely high surface quality and have therefore mainly been restricted to  $\text{Bi}_2\text{Sr}_2\text{CaCu}_2\text{O}_{8+\delta}$ (Bi221) and  $\text{YBa}_2\text{Cu}_3\text{O}_{7-\delta}$ (Y123) materials, both with two  $\text{CuO}_2$  layers per unit cell. Techniques that probe deeper into the sample such as dc transport [4–6], optical conductivity [7–9] and NMR [10] were not only the earliest to show evidence of the pseudogap but have been extended to a much larger variety of materials, including several materials with one  $\text{CuO}_2$ . [6] In all cases evidence for a pseudogap has been reported.

The pseudogap in LSCO as seen by NMR and neutron scattering [11] is rather weak and has led to the suggestion that the existence of the pseudogap in the spin excitation spectrum is only possible in bilayer compounds such as Y123 and  $\text{YBa}_2\text{Cu}_4\text{O}_4$ (Y124). In particular, Millis and Monien attribute the pseudogap (or the spin gap) to strong antiferromagnetic correlations between the planes in the bilayer, which are responsible for a quantum order-disorder transition. [10]

Apart from having only one  $\text{CuO}_2$  layer  $\text{La}_{2-x}\text{Sr}_x\text{CuO}_4$  (LSCO) is also a good model system for the study of doping dependences since it can be doped by the addition of strontium over a wide range: from the underdoped, where  $T_c$  increases with Sr content, to the optimally doped where  $T_c$  reaches its maximum value of  $\approx 40 \text{ K}$  at  $x = 0.17$ , and to the

overdoped region where  $T_c \rightarrow 0$  at  $x = 0.34$ . [6]

The characteristic signatures of the pseudogap state in the dc resistivity [4] are seen clearly in LSCO [6,12]. These are the striking deviations below a temperature  $T^*$  from the high temperature linear resistivity, resulting in a clear break in slope at  $T^*$ . It was found by B. Batlogg *et al.* [6] that in LSCO  $T^*$  decreases from 800 K to approximately 300 K as the doping level is increased from the strongly underdoped to just over the optimal doping level. Similar behavior at  $T = T^*$  has been observed in the Hall effect coefficient and the magnetic susceptibility. [13,14]

The pseudogap can also be observed if the conductivity is measured in the frequency domain,  $\sigma(\omega)$ , where it shows up as a striking depression of the frequency dependent scattering rate at low frequency. It is found that below a frequency  $\Omega_p \approx 600 \text{ cm}^{-1}$ , the scattering rate drops below its high temperature, high frequency, linear behavior. This effect has been clearly identified in the bilayer materials. [7–9] One of the aims of this paper is to see if this behavior can also be observed in LSCO. A pseudogap state can be defined in terms of this suppression of scattering: the material is in the pseudogap state when the scattering rate falls below the high frequency straight-line extrapolation. In the low frequency limit the scattering rate is proportional to the dc resistivity. Due to this, the  $1/\tau(\omega, T)$  suppression should be compared to the suppression of  $\rho_{DC}(T)$  [6] at temperatures below the linear T dependence region. The IR measurement gives us the possibility to see both the frequency and the temperature dependence of this feature.

A pseudogap feature can also be observed in the  $c$ -

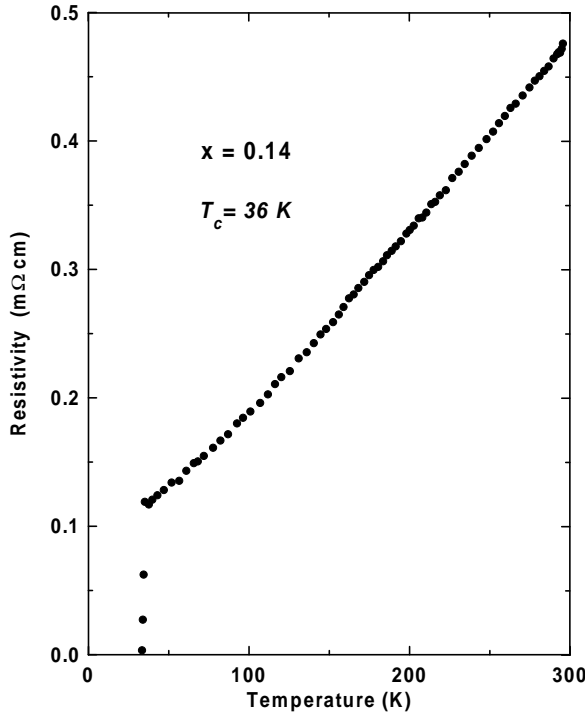


FIG. 1. The temperature dependence of the in-plane resistivity of  $\text{La}_{1.86}\text{Sr}_{0.14}\text{CuO}_4$  is shown with a sharp superconducting transition at 36 K. The shape of the curve is consistent with  $T^*$  being greater than 300 K.

axis IR conductivity in the form of a gap-like region of depressed conductivity at low frequency. It has been reported in  $\text{YBa}_2\text{Cu}_3\text{O}_{7-x}$  (Y123) and  $\text{YBa}_2\text{Cu}_4\text{O}_8$  (Y124) materials [7,15] as well as in LSCO [16,17]. In slightly underdoped LSCO the pseudogap state in the  $c$ -axis direction is not as well defined as it is in the two plane materials. [7] However, as the doping is reduced further, the  $c$ -axis pseudogap state features below 0.1 eV become clearer. [17]

Previous work on the in-plane  $\sigma(\omega)$  of the single layer lanthanum strontium cuprate includes work on the oxygen doped  $\text{La}_2\text{CuO}_{4-\delta}$  [18], thin films of LSCO [19] as well as work done on LSCO single crystal at room temperature [12]. To our knowledge, a study of the temperature and doping dependence has not been done. We fill this gap here by performing optical measurements on high-quality LSCO single crystals at temperatures ranging from 10 K to 300 K at two different doping levels, both slightly underdoped. Also the optical properties of both the ab-plane and  $c$ -axis of  $\text{La}_{1.87}\text{Sr}_{0.13}\text{CuO}_4$  were measured on the same crystal.

To better display the effect of increased coherence on  $\sigma(\omega)_{ab}$  resulting from the formation of the pseudogap state we use the memory function, or extended Drude analysis. In this treatment the complex optical conductivity is modeled by a Drude spectrum with a frequency-

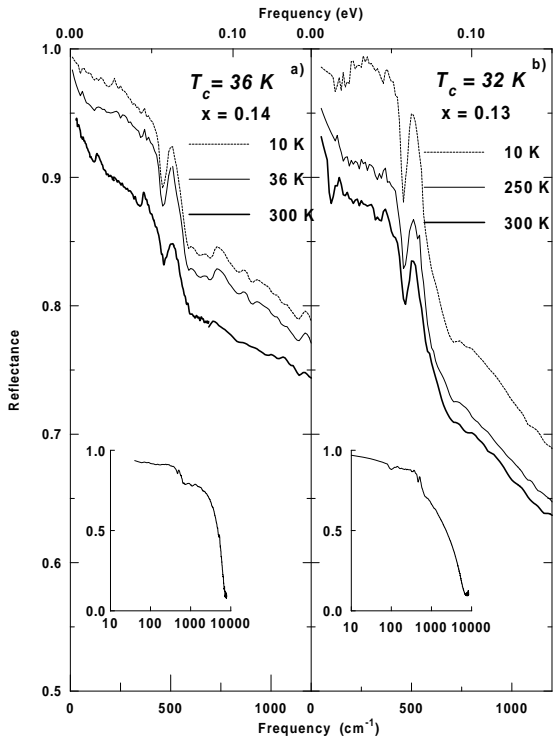


FIG. 2. The reflectance of  $\text{La}_{1.86}\text{Sr}_{0.14}\text{CuO}_4$  (a) and  $\text{La}_{1.87}\text{Sr}_{0.13}\text{CuO}_4$  (b) is shown. The solid lines show normal state spectra, the dashed curve shows superconducting state spectrum. The thinnest line shows the spectrum at the temperature closest to  $T_c$ . The insert in the left panel is a semi-log graph of the reflectance at 300 K which shows a plasma edge around  $7000 \text{ cm}^{-1}$ .

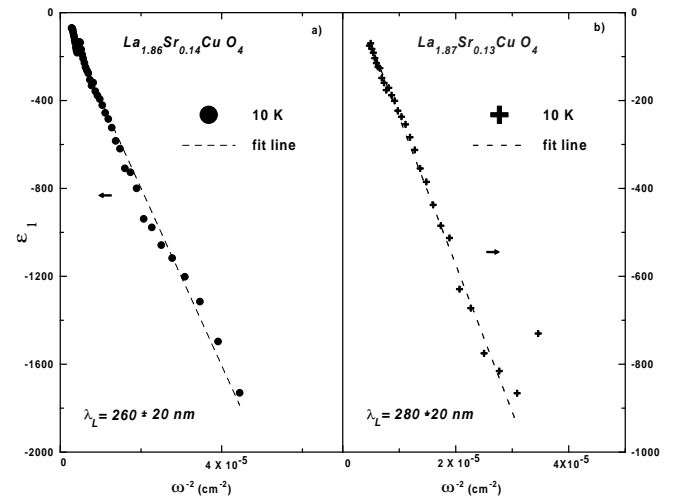


FIG. 3. The real part of the dielectric function as a function of  $\omega^{-2}$  of  $\text{La}_{1.86}\text{Sr}_{0.14}\text{CuO}_4$  at 10 K is shown in the panel a) and of  $\text{La}_{1.87}\text{Sr}_{0.13}\text{CuO}_4$  at 25 K is shown at the panel b). The dash line is linear fit. The slope of the fit gives the values of the London penetration depth.

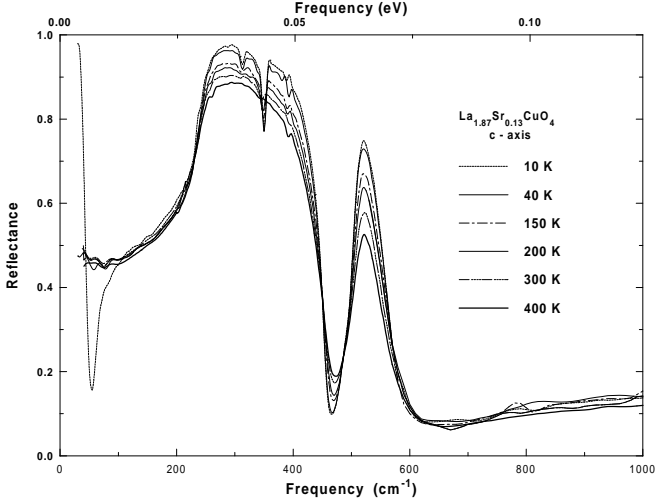


FIG. 4. The reflectance of  $\text{La}_{1.87}\text{Sr}_{0.13}\text{CuO}_4$  with  $E \parallel c$  axis is shown. The temperature sequences are 10 K, 40 K, 150 K, 200 K, 300 K and 400 K

dependent scattering rate and an effective electron mass. [20,21] While the optical conductivity tends to emphasize free particle behavior, a study of the frequency dependence of the effective scattering rate puts more weight on displaying the interactions of the free particles with the elementary excitations of the system. [22] The temperature evolution of the frequency dependent scattering rate and effective mass spectra are of particular interest and are defined as follows:

$$1/\tau(\omega, T) = \frac{\omega_p^2}{4\pi} \text{Re}(\frac{1}{\sigma(\omega, T)}) \quad (1)$$

$$\frac{m^*(\omega, T)}{m_e} = \frac{1}{\omega} \frac{\omega_p^2}{4\pi} \text{Im}(\frac{1}{\sigma(\omega, T)}) \quad (2)$$

Here,  $\sigma(\omega, T) = \sigma_1(\omega, T) + i\sigma_2(\omega, T)$  is the complex optical conductivity and  $\omega_p$  is the plasma frequency of the charge carriers.

The single crystals of  $\text{La}_{2-x}\text{Sr}_x\text{CuO}_4$  with approximate dimensions  $5 \times 3 \times 3$  mm<sup>3</sup> were grown by the traveling-solvent floating zone technique at Oak Ridge [23] in the case of  $x = 0.14$  and in Tokyo [24] in the case of  $x = 0.13$ . The critical temperature was determined by both SQUID magnetization and resistivity measurements and was found to be 36 K for the nominal concentration of Sr  $x = 0.14$  and 32 K for  $x = 0.13$ . Since the highest  $T_c$  in the LSCO system has been found to be 40 K for  $x = 0.17$ , we conclude that both crystals are underdoped.

The crystal with  $x = 0.14$  was aligned using Laue diffraction and polished parallel to the  $\text{CuO}_2$  planes. The crystal with  $x = 0.13$  was polished in Tokyo to yield both ab-plane and ac-plane faces. Both surfaces were measured. Polarizers were used for the ac-face data to

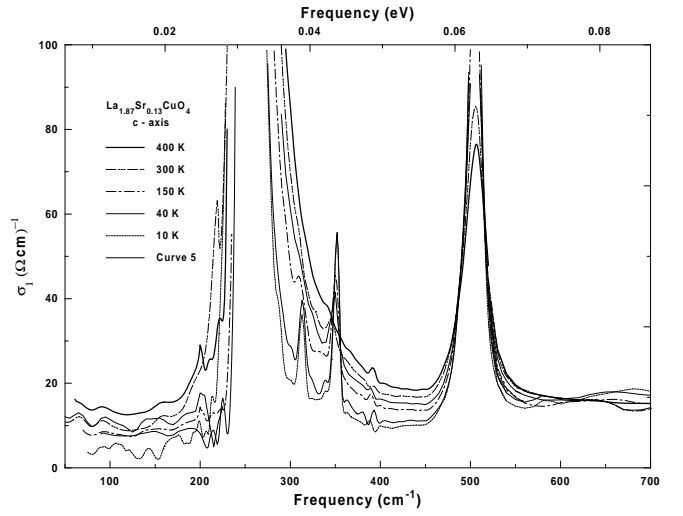


FIG. 5. The c-axis conductivity of the  $\text{La}_{1.87}\text{Sr}_{0.13}\text{CuO}_4$  is shown at different temperatures. Since the phonon peaks are dominant in the direction perpendicular to  $\text{CuO}_2$  planes, the graph is focused at the background conductivity. Two inserts are the c-axis conductivity of the underdoped  $\text{La}_{1.87}\text{Sr}_{0.13}\text{CuO}_4$  measured at  $450 \text{ cm}^{-1}$  and at  $600 \text{ cm}^{-1}$ . The c-axis conductivity at  $450 \text{ cm}^{-1}$  is depressed below 300 K, however, it is somewhat constant above  $600 \text{ cm}^{-1}$ . This could be a signature of the pseudogap formation at the temperatures less than 300 K and with the size of  $500 \text{ cm}^{-1}$ .

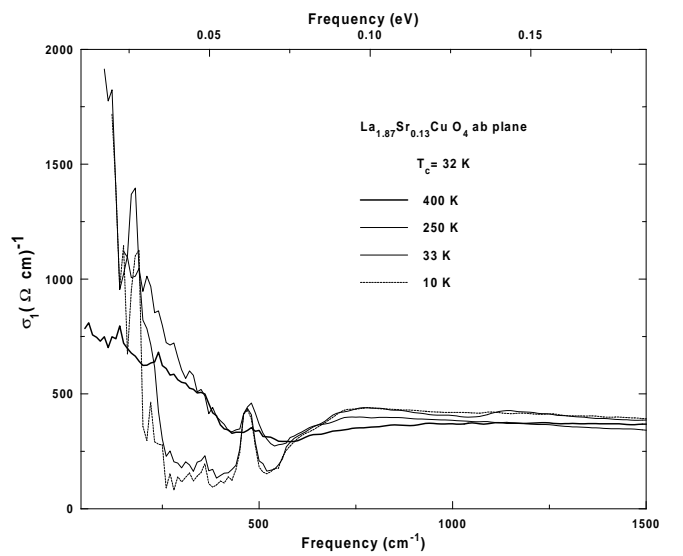


FIG. 6. The ab-plane conductivity of the  $\text{La}_{1.87}\text{Sr}_{0.13}\text{CuO}_4$  is shown at different temperatures.

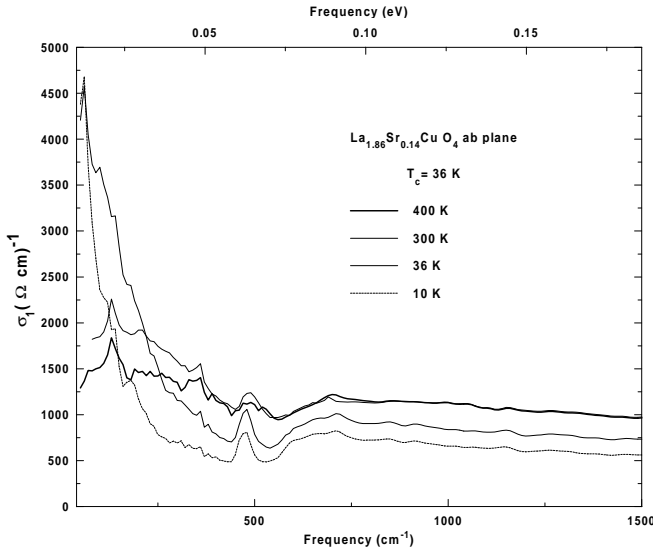


FIG. 7. The ab-plane conductivity of  $\text{La}_{1.86}\text{Sr}_{0.14}\text{CuO}_4$  is shown at different temperatures.

separate the contribution of  $\text{CuO}_2$  planes from the c-axis optical response.

To get an uncontaminated ab-plane measurement, it is important to have the sample surface accurately parallel to the *ab*-plane to avoid any c-axis contribution to the optical conductivity. [25] The miscut angle between the polished surface normal and the c-axis was checked by a high precision triple axis x-ray diffractometer and was determined to be less than 0.8%.

All reflectivity measurements were performed with a Michelson interferometer using three different detectors which cover frequencies ranging from 10 to  $10000\text{ cm}^{-1}$  ( $1.25\text{ meV} - 1.25\text{ eV}$ ). The experimental uncertainty in the reflectance data does not exceed 1%. The dc resistivity measurements were carried out using a standard 4-probe technique.

The result of the resistivity measurement on the same  $\text{La}_{1.86}\text{Sr}_{0.14}\text{CuO}_4$  single crystal used in the optical measurements is shown in Fig. 1. It is commonly accepted that the DC-resistivity is linear at high temperatures for LSCO and that the pseudogap begins to form near the temperature where the resistivity drops below this linear trend. [6] At lower temperatures there is a region of superlinear temperature dependent resistivity. The  $T^*$  value for our samples with  $x = 0.13$  and  $x = 0.14$  extracted from the phase diagram of Batlogg *et al.*, [6] are 650 K and 450 K, respectively. In agreement with this, the resistivity shows a superlinear temperature dependence below room temperature as expected in the pseudogap region.

In Fig. 2 we present the reflectivity data at temperatures above and below  $T_c$  for the two samples. For clarity, only three temperatures are shown:  $T = 300\text{ K}$ , an intermediate temperature above the superconducting

transition and a low temperature  $\approx 10\text{ K}$  in the superconducting state. In the frequency region shown the reflectance is strongly temperature dependent for both materials, dropping by approximately 10% as temperature is increased from the lowest temperature to  $T = 300\text{ K}$ . The plasma edge is observed at  $7800\text{ cm}^{-1}$  (see insert of Fig. 2). The distinct peaks at approximately 135 and  $365\text{ cm}^{-1}$  in the LSCO reflectivity spectra correspond to the excitation of ab-plane *TO* phonons and the peak at  $500\text{ cm}^{-1}$  corresponds to a *LO* phonon. [26] As in all other HTSC materials, the ab plane has a coherent response with very high reflectance.

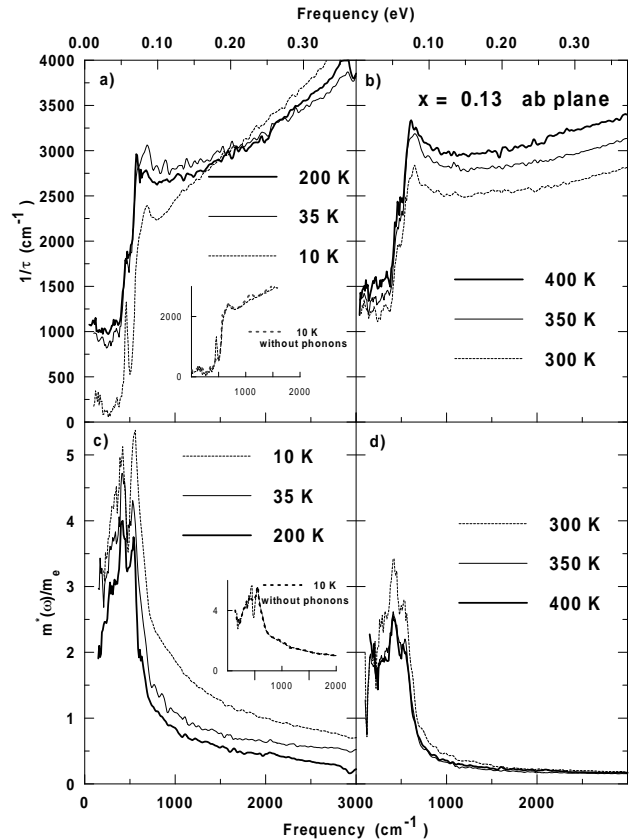


FIG. 8. Top panel: the low temperature frequency dependent scattering rate of  $\text{La}_{1.87}\text{Sr}_{0.13}\text{CuO}_4$  below  $T^{**}$ (a) and above  $T^{**}$ (b) is calculated using Equation (1). The onset of the suppression in a conductivity corresponds to a drastic change in the frequency dependence of the scattering rate below  $T^*$ . Above  $700\text{ cm}^{-1}$  the scattering rate is nearly temperature independent and has a linear frequency dependence below  $T^{**}$ . Below  $700\text{ cm}^{-1}$  the scattering rate varies as  $\omega^{1+\delta}$  and shows a strong temperature dependence. Bottom panel: The effective mass of  $\text{La}_{1.87}\text{Sr}_{0.13}\text{CuO}_4$  below  $T^{**}$ (a) and above  $T^{**}$ (b) is calculated using Equation (2). The onset of enhancement of  $\frac{m^*(\omega)}{m_e}$  corresponds to the onset of the suppression of the scattering rate.

The complex optical conductivity  $\sigma(\omega)$  was obtained by Kramers-Kronig analysis of the reflectivity data.

Since, in principle, this analysis requires knowledge of the reflectance at all frequencies, reflectivity extensions must be used at high and low frequencies. The Hagen-Rubens formula was used for the low frequency reflectivity extrapolation, with parameters taken from the dc resistivity measurements on the same sample with  $x = 0.14$  shown in Fig. 1 and the results of H. Takagi *et al.* [27] for the sample with  $x = 0.13$ . For the high-frequency expansion for  $\omega > 8000 \text{ cm}^{-1}$  we used the reflectivity result Uchida *et al.* [12]. At frequencies higher than 40 eV reflectivity was assumed to fall as  $1/\omega^4$ .

We calculate the plasma frequency of the superconducting charge carriers and the London penetration depth using the following formula: [28]

$$\epsilon_1 = 1 - \frac{\omega_{ps}^2}{\omega^2}.$$

The slope of the low-frequency dielectric function  $\epsilon_1(\omega)$ , plotted as a function of  $\omega^{-2}$  in Fig. 3a,b, gives plasma frequencies of  $6100 \text{ cm}^{-1}$  and  $5700 \text{ cm}^{-1}$  in superconducting state. The corresponding London penetration depths are  $\lambda_L = 1/2\pi\omega_{ps} = 250 \text{ nm}$  and  $280 \text{ nm}$  for  $\text{La}_{1.86}\text{Sr}_{0.14}\text{CuO}_4$  and  $\text{La}_{1.87}\text{Sr}_{0.13}\text{CuO}_4$ , respectively. These values are in good agreement with those obtained previously by Gao *et al.* in films [19] ( $\lambda_L = 275 \pm 5 \text{ nm}$ ) and by muon-spin-relaxation [29] ( $\lambda_L = 250 \text{ nm}$ ).

The c-axis reflectance of the  $x = 0.13$  sample is shown in Fig. 4. The corresponding conductivity is low and dominated by optical phonons (Fig. 5).

In YBCO 123 and 124 the pseudogap in c-axis conductivity manifests itself as a depression in conductivity at low frequency. [15,7,30] There is no coherent Drude tail and the conductivity is flat and frequency independent. In the temperature and doping range where a pseudogap is expected a low frequency depression of conductivity is seen with an edge in the  $300\text{--}400 \text{ cm}^{-1}$  region where conductivity rises to the high frequency plateau.

In order to isolate the electronic features of our LSCO c-axis spectrum we magnify the low value region of (Fig. 5). There is no sharp pseudogap edge in the low frequency infrared data for underdoped LSCO as there is in the case of Y123. It is possible that such a feature could be hidden under the large phonon structure. Efforts to subtract the phonons in order to extract the background conductivity were found to be extremely sensitive to the choice of their shape in fitting procedures. Nonetheless, the raw data clearly show that there is a low frequency depression of the c-axis conductivity. Conductivity at  $450 \text{ cm}^{-1}$  is uniformly suppressed below  $T=300 \text{ K}$  (Fig. 5 insert), whereas the conductivity at  $600 \text{ cm}^{-1}$  is nearly constant at all temperatures. Based on this analysis one can conclude that the pseudogap state in the c-axis opens up below  $300 \text{ K}$  and its size is approximately equal to  $500 \text{ cm}^{-1}$ .

Manifestations of the pseudogap in the *ab*-plane conductivity exist as a loss of spectral weight between  $700$

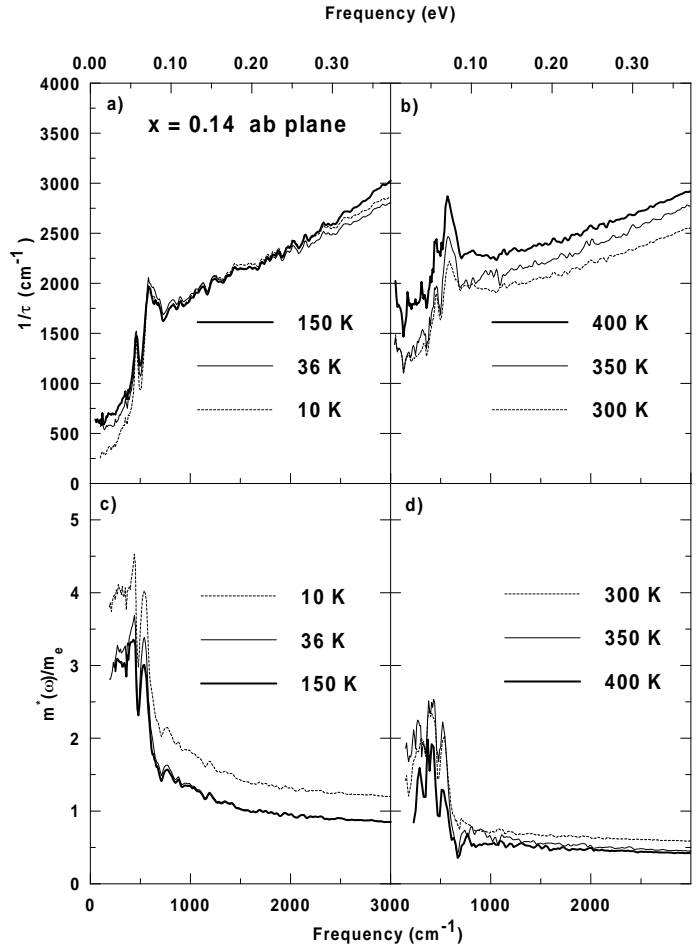


FIG. 9. Top panel: the high temperature effective scattering rate of  $\text{La}_{1.86}\text{Sr}_{0.14}\text{CuO}_4$  below  $T^{**}$  (a) and above  $T^{**}$  (b) is calculated using Equation (1). Above  $700 \text{ cm}^{-1}$  the scattering rate has a linear frequency and temperature independent below  $T^{**}$  (a) and temperature dependent above  $T^{**}$  (b). Below  $700 \text{ cm}^{-1}$  the scattering rate varies as  $\omega^{1+\delta}$  and shows a strong temperature dependence. Bottom panel: The effective mass of  $\text{La}_{1.87}\text{Sr}_{0.13}\text{CuO}_4$  below  $T^{**}$  (a) and above  $T^{**}$  (b) samples is calculated using Equation (2).

and  $200 \text{ cm}^{-1}$  balanced by increases both below and above this frequency. In both Fig. 6 and Fig. 7 one can see the temperature evolution of the sharp depression in  $ab$ -conductivity below  $700 \text{ cm}^{-1}$  at temperatures above  $T_c$ . A much clearer picture of the pseudogap state can be seen from the effective scattering rate,  $1/\tau(\omega, T)$ , calculated from the conductivity using equation (1) which is shown along with the effective mass in Fig. 8 and Fig. 9. The  $1/\tau(\omega, T)$  spectra can conveniently be divided into two regions. In the high frequency region, starting at about  $700 \text{ cm}^{-1}$ , the scattering rate varies linearly with frequency while in the low frequency region there is a clear suppression of  $1/\tau(\omega, T)$  below this linear trend. [31] The temperature where this suppression first appears serves as a definition of  $T^*$ , the onset temperature of the pseudogap state. As the temperature is lowered below  $T^*$  this suppression becomes deeper. We find that for underdoped  $\text{La}_{2-x}\text{Sr}_x\text{CuO}_4$   $T^* \geq 400 \text{ K}$ , an order of magnitude higher than the superconducting transition temperature  $T_c$  (32 K). This is significantly different from previous results on cuprates where  $T^*$  more or less coincides with  $T_c$  near optimal doping.

The temperature dependence above  $700 \text{ cm}^{-1}$  is strongly influenced by the level of Sr doping. In the underdoped sample the high frequency scattering rate is nearly temperature independent up to a certain temperature (Fig. 8a and Fig. 9a), which we will call  $T^{**}$  above which a pronounced temperature dependence of  $1/\tau(\omega, T)$  is seen (Fig. 8b and Fig. 9b). In the  $x = 0.13$  sample  $T^{**} \approx 200 \text{ K}$  while in the  $x = 0.14$  sample  $T^{**} \approx 150 \text{ K}$ . In the overdoped samples the scattering rate above  $700 \text{ cm}^{-1}$  increases uniformly with temperature [32] at all temperatures suggesting  $T^{**} \rightarrow 0$  in that limit. This behavior is also seen in other overdoped HTSC. [31]

If one extrapolates the 300 K scattering rates to zero frequency one finds that for the  $x = 0.13$  sample the scattering rate  $1/\tau_0 \approx 2500 \text{ cm}^{-1}$  and for the  $x = 0.13$  sample this rate is  $\approx 1500 \text{ cm}^{-1}$ . These scattering rates are much higher than what is seen for the higher  $T_c$  materials reviewed by Puchkov *et al.* [31] where at 300 K  $1/\tau_0 \approx 1000 \pm 200 \text{ cm}^{-1}$  for several families and many doping levels. This high residual scattering differentiates the LSCO material from the other cuprates.

If we call the frequency below which the scattering rate is suppressed the  $ab$ -plane pseudogap  $\omega_{ab} \approx 700 \text{ cm}^{-1}$  we find it is clearly bigger than the  $c$ -axis pseudogap frequency  $\omega_c \approx 500 \text{ cm}^{-1}$

In addition to the pseudogap depth and temperature dependence, several other features of Figures 8 and 9 should be mentioned. The position of the pseudogap remains at  $700 \text{ cm}^{-1}$  for all temperatures. There are also several peaks positioned at  $500 \text{ cm}^{-1}$  in the scattering rate which complicate the analysis, particularly in the case of the sample with  $x = 0.14$ . These peaks have been observed by other groups and have been attributed to po-

laronic effects. [33,34] Another possible explanation is the correlation of the  $ab$ -plane conductivity with  $c$ -axis LO phonons. We did observe the difference in contribution of LO phonons to the  $ab$  plane reflectance with different propagation directions, an effect first observed by Reedyk *et al.*, [35] and also seen in the  $k \parallel c$  vs.  $k \perp c$  spectra obtained by Tanner's group. [18] In Fig. 10 the reflectance with  $E \parallel a$  and  $k \parallel c$ , is compared with the reflectance with  $E \parallel ab$  and  $k \parallel a$ , with the  $\text{La}_{1.87}\text{Sr}_{0.13}\text{CuO}_4$  sample at room temperature. There is an extra feature observed at  $500 \text{ cm}^{-1}$  in the spectra with  $k \parallel c$ . Further evidence that the  $c$ -axis LO phonons couples to  $ab$  plane features can be seen in Fig. 11. The comparison between peaks in the effective scattering rate at  $450 \text{ cm}^{-1}$  and  $580 \text{ cm}^{-1}$  to the peaks in  $\text{Im}(-1/\epsilon_c)$  shows the same strong correlation seen in many other cuprates. [35]

For completeness we also plot the effective mass of underdoped samples at low temperatures (Fig. 8c) and high temperatures (Fig. 9c,d). As expected,  $\frac{m^*(\omega)}{m_e}$  rises to a maximum  $\approx 3$  forming a peak at  $\approx 400 \text{ cm}^{-1}$ . The enhancement of the effective mass in the pseudogap state as well as the upper limit of  $\frac{m^*(\omega)}{m_e}$  are similar to what has been previously reported for Y123, Y124 and Bi2212. [31]

Before closing we compare our results with data of Gao *et al.* [19] on  $\text{La}_{2-x}\text{Sr}_x\text{CuO}_{4+\delta}$  films and Quijada *et al.* [18] on oxygen doped  $\text{La}_2\text{CuO}_{4+\delta}$ . Our results in the underdoped case are comparable with those of the oxygen doped material, although Quijada *et al.* did not carry out a frequency dependent scattering rate analysis for their underdoped sample. The film results of Gao *et al.* are quite different from our findings. The films used in that study had a strontium level that would correspond to optimal doping in crystals. However, the  $1/\tau(\omega)$  curves deviate markedly from what we observe for slightly under and overdoped samples. The authors performed an extended Drude analysis and found a strongly temperature dependent scattering rate even at low temperatures. This is in sharp contrast to our results which would suggest a very weak temperature dependence in this temperature region. Based on our work, their samples should be in the pseudogap state since they have an  $x$  value near optimal doping. Comparing these results with other systems, in particular with Tl2202, two factors suggest the possibility that the films may be overdoped. First, their  $T_c$  was near 30 K, lower than that expected for optimal doping. Secondly, it is known that the oxygen level in films can vary substantially and in LSCO oxygen can have a major influence on the doping level [36]. On the other hand, we cannot completely rule out the possibility that all the crystal results are affected by the polishing process, and that the films better represent the bulk material. It is clearly important to measure films where the oxygen content is controlled by selective annealing.

In conclusion, the optical data in the far-infrared re-

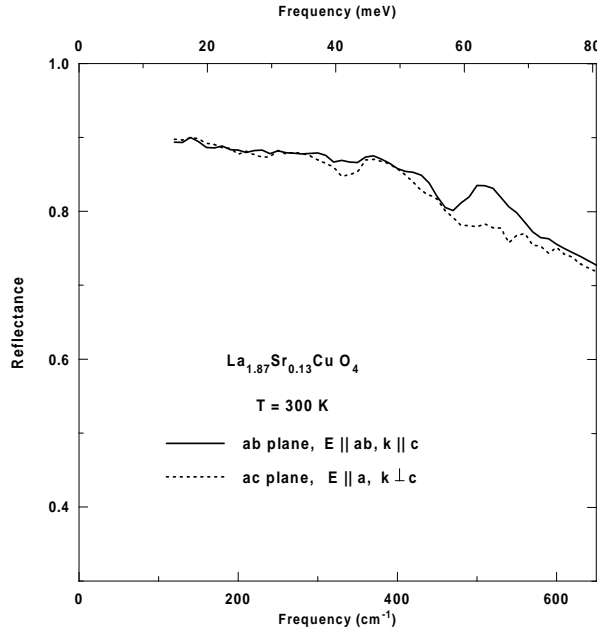


FIG. 10. Comparison of the reflectance of  $\text{La}_{1.87}\text{Sr}_{0.13}\text{CuO}_4$  measured from ab plane with  $k \parallel c$  and from ac plane with  $k \perp c$ .

gion, taken on two underdoped *single-layered* high- $T_c$  superconductors, shows clear evidence of a *pseudogap state* in both the scattering rate and conductivity along  $\text{CuO}_2$  planes. This pseudogap state extends to higher temperatures than that observed in the multi-layered underdoped cuprates such as YBCO and BSCO.

The scattering rate is similar for both systems in the pseudogap state. At low frequencies,  $\omega \leq 700 \text{ cm}^{-1}$ , the scattering rates are *temperature* dependent and change with frequency in a *non-linear* fashion. Above  $700 \text{ cm}^{-1}$  this behavior becomes *linear*. Within experimental uncertainty the observed high frequency scattering rate of the underdoped sample is *not affected by temperature* up to certain temperature  $T^{**}$ . This temperature is equal to 200 K in case of  $\text{La}_{1.87}\text{Sr}_{0.13}\text{CuO}_4$  and 150 K in case of  $\text{La}_{1.86}\text{Sr}_{0.14}\text{CuO}_4$ . Above  $T^{**}$  the high frequency scattering rate is temperature dependent. This behavior is identical to the high-frequency effective scattering rate of an overdoped HTSC. [31]

Our findings in the direction perpendicular to the  $\text{CuO}_2$  planes showed that the depression of the c-axis conductivity is not as prominent as the one found in the two layer HTSC. Nevertheless, the signature of the pseudogap can be seen at the frequencies below  $500 \text{ cm}^{-1}$  up to room temperature.

We would like to thank J.D. Garrett for help in aligning the sample and also P.C. Mason, M. Lumsden and B.D. Gaulin for determining the miscut angle of the underdoped LSCO crystal. We also take this opportunity to thank K.C. Irwin and J.G. Naeini for their useful collaboration. This work was supported by the Natural Sci-

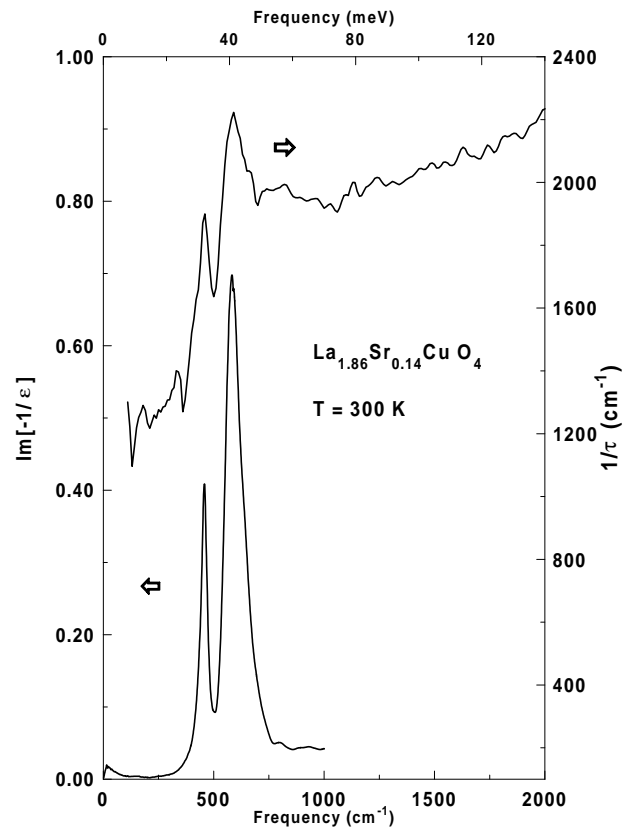


FIG. 11. Comparison of the peaks position at  $450$  and  $580 \text{ cm}^{-1}$  in the dielectric loss function of the c-axis phonons with the effective scattering rate of  $\text{La}_{1.86}\text{Sr}_{0.14}\text{CuO}_4$  at room temperature. The correspondence of the peaks positions, width and the relative strength suggests that the nature of the peak may lie in the coupling of a ab-plane spectra to the c-axis longitudinal optical phonons.

---

[1] T. Timusk and B. Statt, Rep. Prog. Phys. (to be published).

[2] D.S. Marshall, A.G. Loeser, Z.-X. Chen, and D.S. Dessau, Physica C, **263**, 208 (1999).

[3] H.J. Tao, F. Lu, and E.L. Wolf, Physica C **282-287**, (1987); Ch. Renner, B. Revaz, J.-Y. Genoud, K. Kadrowaki, and O. Fischer, Phys. Rev. Lett. **80**, 149, (1998).

[4] B. Bucher, P. Steiner, J. Karpinski, E. Kaldis, and P. Wachter, Phys. Rev. Lett. **70**, 2012, (1993).

[5] T. Ito, K. Takenaka, and S. Uchida, Phys. Rev. Lett. **70**, 3995, (1993).

[6] B. Batlogg, H.Y. Hwang, H. Takagi, R.J. Cava, H.L. Kao, and J. Kuo, Physica C, **235-240**, 130 (1994).

[7] D.N. Basov, R. Liang, B. Dabrowski, D.A. Bonn, W.N. Hardy, and T. Timusk, Phys. Rev. Lett., **77**, 4090 (1996).

[8] A.V. Puchkov, P. Fournier, D.N. Basov, T. Timusk, A. Kapitulnik, and N.N. Kolesnikov, Phys. Rev. Lett., **77**, 3212 (1996).

[9] A.V. Puchkov, P. Fournier, T. Timusk, and N.N. Kolesnikov, Phys. Rev. Lett., **77**, 1853 (1996).

[10] A.J. Millis and H. Monien, Phys. Rev. Lett., **70**, 2810 (1993).

[11] T.E. Mason, G. Aeppli, and H.A. Mook, Phys. Rev. Lett., **68**, 1414 (1992).

[12] S. Uchida, I. Ido, H. Takagi, T. Arima, Y. Tokura, and S. Tajima, Phys. Rev. B **43**, 7942 (1991).

[13] H.Y. Hwang, B. Batlogg, H. Tagaki, H.L. Kao, J. Kwo, R.J. Cava, and J.J. Krajewski, Phys. Rev. Lett., **72**, 2636 (1994).

[14] S.K. Tolpygo, J.-Y. Lin, M. Girvich, S.Y. Hou, and Julia M. Phillips, Phys. Rev. B, **53**, 12454 (1996).

[15] C.C. Homes, T. Timusk, R. Liang, D.A. Bonn, and W.N. Hardy, Phys. Rev. Lett., **71**, 1645 (1993).

[16] D.N. Basov, R. Liang, B. Dabrowski, D.A. Bonn and W.N. Hardy, T. Timusk, Phys. Rev.B, **52**, R13141 (1995).

[17] S. Uchida, K. Tamasaky, and S. Tajima, Phys. Rev.B, **53**, 14558 (1996).

[18] M.A. Quijada, D.B. Tanner, F.C. Chou, D.C. Johnston and S.-W. Cheong, Phys. Rev. B, **52**, 15485 (1995).

[19] F. Gao, D.B. Romero, B.D. Tanner, J. Talvacchio, and M.G. Forrester, Phys. Rev.B, **47**, 1036 (1993).

[20] W. Götze and P. Wolfle, Phys. Rev.B, **6**, 1226 (1972).

[21] P.B. Allen, Phys. Rev.B, **3**, 305 (1971).

[22] A. Gold, S.J. Allen, B.A. Wilson and D.C. Tsui, Phys. Rev.B, **25**, 3519 (1982).

[23] S.-W. Cheng, G. Aeppli, T.E. Mason, H. Mook, S.M. Hayden, P.C. Canfield, Z. Fisk, K.N. Clausen, and J.L. Martinez, Phys. Rev. Lett., **67**, 1791 (1991).

[24] T. Kimura, K. Kishio, T. Kobayashi, Y. Nakayama, N. Motohira, K. Kitazawa, and K. Yamafuji, Physica C(Amsterdam), **192**, 247 (1992).

[25] J. Orenstein and D.H. Rapkine, Phys. Rev. Lett., **60**, 968 (1988).

[26] S. Tajima, S. Uchida, S. Ishibashi, T. Ido and H. Takagi, T. Arima and Y. Tokura, Physica C, **168**, 117 (1990).

[27] H. Takagi, B. Batlogg, H.L. Kao, J. Kwo, R.J. Cava, J.J. Krajewski, and W.F. Peck, Jr., Phys. Rev. Lett., **69**, 2975 (1992).

[28] D.B. Tanner and T. Timusk, in *Physical Properties of High Temperature Superconductors I*, edited by D.M. Ginsberg (word Scientific, Singapore, 1992), p.363.

[29] G. Aeppli, R.J. Cava, E.J. Ansaldi, J.H. Brewer, S.R. Kreitzman, G.M. Luke, D.R. Noakes, and R.F. Kiefl, Phys. Rev. B, **35**, 7129 (1987).

[30] C.C. Homes, T.Timus, R. Liang, D.A. Bonn, and W.H. Hardy, Physica C, **254**, 265-280, (1995).

[31] A.V. Puchkov, D.N. Basov, and T. Timusk, J. Phys.: Condens. Matter, **8**, 10049 (1996).

[32] T. Startseva, T. Timusk, M. Okuya, T. Kimura, and K. Kishio, to be published.

[33] Y. Yagil and E.K.H Salje, Physica C, **235-140**, 1143 (1994).

[34] G.A. Thomas, D.H. Rapkine, S.L. Cooper, S.-W. Cheong, A.S. Cooper, L.S. Schneemeyer, and J.V. Waszczak, Phys. Rev. B, **45**, 2474 (1992).

[35] M. Reedyk, T. Timusk, Phys. Rev. Lett., **69**, 2705 (1992)

[36] H. Zhang, H. Sato, and G.L. Liedl, Physica C **234**, 185, (1994).

[37] T. Timusk, D.N. Basov, C.C Homes, A.V. Puchkov, and M. Reedyk, Journ. of Superconductivity, **8**, 437 (1995).

[38] K. Tamasaku, T. Itoh, H. Takagi, and S. Uchida, Phys. Rev. Lett., **72**, 3088 (1994).

[39] P.A. Lee and N. Nagaosa, Phys. Rev. B, **46**, 5621 (1992).

[40] V.J. Emery and S.A. Kivelson, Phys. Rev. Lett., **74**, 3253 (1995).

[41] J.W. Loram, K.A. Mirza, J.R. Cooper, and W.Y. Liang, Phys. Rev. Lett., **71**, 1740 (1993).